A Computational Effort to Untangling Anti-SARS-CoV-2 Effects of Oleanolic Acid Analogues

Baran Rajaei[1]

[1]Affiliation not available

January 14, 2024

A Computational Effort to Untangling Anti-SARS-CoV-2 Effects of Oleanolic Acid Analogues

Baran Rajaei*

Abstract: Considering urgent need for novel drugs to target severe acute respiratory syndrome coronavirus 2 (SARS-CoV-2), we reported at least four Kurdish ethno-medical, antipyretic recipes which can be translated into functional antiviral formulations. This computational work highlights the implications of oleanolic acid and its analogues as a cluster of binder candidates of SARS-CoV-2 main protease (Mpro). Through molecular docking and simulation, we found oleanolic acid (-12.6 Kcal/mol) and its two analogues (OA11; ligand I [-14.2 Kcal/mol]) and (OA31; ligand II [-14.0 Kcal/mol]) bound with Mpro (PDB: 6Y84) more reliably than saquinavir (-8.1 Kcal/mol), as a canonical drug. Salaspermic acid, (3b)-3-{[(2E)-3-phenylprop-2-enoyl]oxy}olean-12-en-28-oic acid, OA37 and OA40 interacted with catalytic dyad and major amino acid residues of Mpro active sites; these toxic compounds may be future anti-protease drug candidates. This study proposes this set of anti-protease pentacyclic triterpenoids should be assayed against SARS-CoV-2 at in vitro level or in clinical settings.
Keywords: Main Protease; M^{pro}; COVID-19; oleanolic; acid toxicity; computational biology

INTRODUCTION

From December 2019, the world faced with the emergence of a newly-evolved strain of coronavirus known as severe acute respiratory syndrome coronavirus 2 (SARS-CoV-2) which has left an indelible mark upon all aspects of life across the world. The corona-virus disease 2019 (COVID-19) pandemic showed a multi-surge pattern caused by SARS-CoV-2 variants classified as variants of interest, concern and high consequences [3, 4]. The fatality rate of COVID-19 tends to increase during cold weather that may be different to seasonal influenza [5, 6] and common cold [7]. Although, the global vaccination against COVID-19 has progressively been performed, millions of people are still unvaccinated due to poor vaccination coverage in many areas such as poor, populous and developing countries [8, 9].

Corresponding author:
Independent Bioinformatician,
Baranrajaei1990@gmail.com

In any way, our neighbors in the society may be infected and may infect vaccinated or unvaccinated subjects easily due to increased transmissibility of SARS-CoV-2 [10]. As a result, identification or development of anti-viral therapeutic agents and remedies being able to exert therapeutic or prophylactic effects on COVID-19 (especially long form) must be taken into consideration as alternative to available vaccines [11]. Considerably, Kurdish ethnomedicine is a historical heritage belonging to Kurds providing us with an array of phytomedicines, phytobiotics, functional foods, functional teas and functional formulations extensively applied to treat or to prevent numerous pathological conditions such as infectious diseases [12]. Recently, a large number of *in silico* investigations along with experimental efforts reported some drug- and lead-like compounds possibly possessing potent anti-COVID-19 efficacy [13, 14] but the contagious and life-threatening nature of COVID-19 prevents practitioners from routinely assaying compounds in experiments conducted at both *in vitro* and *in vivo* levels. Fortunately, the advancement in computational pharmacology and toxicology can accelerate the process of seeking efficient and potent remedies and reduce the cost of conventional experimentation [15, 16]. In this essence, U.S. Patent. No. 5,178,865 discloses an experimental treatment with 56 herbs and reported that 10 out of 56 herbs exhibited inhibitory effect against human immunodeficiency virus (HIV) in the *in vitro* experiments [17, 18]. These 10 herbs were *Coptis chineusis, Ligusticum wallichii, Ilicium eanclolatum, Isatis tinctoria, Salvia miltiorrhiza, Erycibe obtusifolia, Acanthopanax graciliatylus, Bostaurus domesticus, Inula helenium* and *Lonicera japonica* [18]. Both *Bostaurus domesticus* and *Lonicera japonica* plus *Scutellaria baicaleusis* exhibited strong anti-HIV activity [19, 20]. In the same way, U.S. Patent. No. 5,837, 257 reported that Chinese herbal medicines exhibit anti-viral activity against murine leukemia virus and HIV which was confirmed through *in vitro* studies. As other instances, Chinese herbal antiviral medicines including hedyotis, *Prunellae spica*, *Lonicera flos*, *Scutellaria barbatae herba*, and *Solani harba* have been reported [21]. Accordingly, the present study was aimed at computational discovery of possible antiviral properties of herbal remedies used as antipyretic or anti-flu in Kurdish ethno-medicine and it we tried to identify potential anti-COVID-19 lead-like compounds. In this regard, fenugreek (*Trigonella foenum-graecum*), chamomile (*Matricaria chamomilla*), sage (*Salvia officinalis*) and zingiber (*Zingiber officinale*) have been proposed in various (sole or supplementary) formulations for COVID-19 prophylaxis and therapy in Kurdish ethnomedicine (for a review see [22]). According to initial computational effort, oleanolic acid (OA) showed the most reliable binding affinity (BA; -12.7 Kcal/mol) against SARS-CoV-2 3C-like protease (M^{pro}) among an

array of phytocompounds reported in aforementioned plants. Oleanolic acid, a pentacyclic triterpene (PT), was considered the hit molecule of our first computational effort and here we placed our concentration upon OA and its analogues reported in a seminal paper [1], in order to provide an insightful path to discover anti-SARS-CoV-2 drug- or lead-like compounds. Eventually, multiple studies introduced a number of phytocompounds which may be curative or prophylactic to febrile flu-like conditions occurred in common cold and COVID-19 [23-25]. In a broad view, this study puts forth a great deal of effort to provide a methodological guide on how future pandemics can be managed with the help of ethnopharmacology.

MARTIALS AND METHODS

This study has been focused on the widely used computational tools like molecular docking, molecular dynamics and simulations for the identification of possible binders to SARS-CoV-2 main protease (M^{pro}). The notable steps utilized in the current study has been depicted in fig. 1.

Preparation of target M^{pro} and 42 Analogues of OA

The X-ray crystal structure of M^{pro} was retrieved from PDB Research Collaboratory for Structural Bioinformatics database (http://www.RCSB.org) with ID: 6Y84. It consists of two chains (A and B) containing 309 amino acids with 1.39 Å reported resolution. Alternatively, the chemical structure of OA and its analogues have been curated from PubChem database (https://pubchem.ncbi.nlm.nih.gov/), Drug Bank *ver.* 5.0 (https://www.drugbank.ca/) or drawn using ChemDraw program *ver.* 15.7.13.0 as needed to build up a personal dataset (see fig. 2).

Preparation of binders and protein

The target protein, M^{pro} (PDB: 6Y84), have been prepared using Molegro Virtual Docker (Thomsen and Christensen, 2006) and Chimera 1.8.1 (http://www.rbvi.ucsf. edu/chimera) before trying docking step. The computational molecular docking of phytocompounds (*vide supra*) and druggable protein M^{pro} was accomplished by VINA WIZARD module launched on PyRx programming adaptation 0.8 [26]. The study revealed the final score of sub-atomic docking expressed in BA (Kcal/mol) for a set of docked molecule poses. The maximum exhaustiveness (n = 80) was calculated for each ligands and maximum VINA search space has been selected for docking box to cover whole protein and accommodate ligand to search freely and hit the best binding site in PyRx. The ligand-protein interaction in VINA WIZARD has been scored based on the estimated ligand-protein free energy of the binding (BA, ΔG, Kcal/mol). The binders possessing the strongest BA for 6Y84 were submitted to molecular dynamics (*vide infra*). The best posed ligands docked with 6Y84 were prepared using Chimera 1.8.1 (http://www.rbvi.ucsf. edu/chimera) and Molegro Virtual Docker [27]. These computational tools have also been employed to prepare protein and library files. The pose docking analysis and graphical interface of shortlisted compounds with M^{pro} were dissected using LigPlot^{+} programming to recognize amino acid residues which are involved in the chemical interactions [28]. Conventionally, the binders that demonstrated BA less than -7.0 Kcal/mol were identified as reliable binders with M^{pro} and were discussed (*vide infra*).

Analysis of pharmaco- and toxico-kinetic parameters

Physico-chemical properties and computational descriptors of absorption, distribution, metabolism and excretion (ADME) for acknowledged compounds were evaluated using Swiss ADME program (http://www. swissadme.ch/). This online tool precisely predicts a plethora of pharmaco-kinetic properties including dissolvability, log P, pKa and cytochrome P450 (CYP) interaction and offers violations of Lipinski's rule of five to predict drug-likeness of binders of interest [29]. Furthermore, Toxtree software platform v2.5.1 (http://toxtree.sourceforge.net/) was employed to predict the toxicity class of phytocompounds when administered orally based on their molecular structure [30]. In this scenario, there exist low (class I) substances with simple chemical structures which efficient metabolic modes exist for them, suggesting a low order of oral toxicity. Fifth percentile NOEL (no observable effect level; mg/kg body weight/day) of 3.0 and human exposure threshold (mg/person/day) of 1.8 were considered for this class; intermediate (class II) substances possessing structures which are less innocuous compared to class I substances, but not containing structural features suggestive of toxicity like those substances in class III. Fifth percentile NOEL (mg/kg body weight /day) of 0.91 and human exposure threshold (mg/person/day) of 0.54 were considered for this class; and high (class III) substances with chemical structures permitting no strong initial presumption of safety or may even suggest significant toxicity or have reactive functional groups. Fifth percentile NOEL (mg/kg body weight /day) of 0.15 and human exposure threshold (mg/person/day) of 0.09 were considered for this class [31-33].

Molecular dynamics (MD) studies and trajectories analysis

The stability and movement of top-ranked OA analogues possessed the strongest BA with M^{pro} were evaluated through MD simulation using the GROMACS 2018.8 package [34] and employing the CHARMM36 force field [35]. The conformers with the fittest and lowest docking energy were selected for validation of initial complex interactions. Complete simulation system was placed in a dodecahedron box and water molecules were added using a simple point charge model [36]. To ensure the overall

charge neutrality of the simulated system, sufficient amount of Na^+ counter-ions were added with periodic boundary conditions applied in all three directions of space. The force field parameters of ligands were achieved from CGenFF web server (https://cgenff.umaryland.edu/) [37]. Initially, energy minimization of complex was achieved using the steepest descent method [38]. The procedure of position restraint was accomplished in both NVT and NPT ensembles after energy minimization. The first phase of equilibration involved simulating for 1 ns under the canonical ensemble (NVT) followed by a 1 ns NPT equilibration. The temperature was maintained at 300 °K with the Nose–Hoover thermostat [39-41]. The NPT equilibration was performed using the Parrinello-Rahman barostat [42] to maintain a constant pressure of 1.0bar. In this study, the Lennard-Jones potential with 1.0-nm cutoff, particle mesh Ewald method with 1.0-nm cutoff [43, 44], and the Lincs algorithm [45] were used for van der Waals interactions, long range electrostatics, and covalent bond constraints, respectively. Finally, 100 ns MD simulations was performed to analyze the trajectories using the leap-frog algorithm and solve the equations of motion with a time step of 2 fs.

RESULTS

Molecular docking analysis

Docking study has been pursued to analyze the binding interaction of OA and its analogues to M^{pro} and to predict the general binding modes of ligand for determining the residues of protein which were involved in ligand binding. It has been highlighted that the crucial amino acids of M^{pro} were involved in the stable interaction of respective ligands or control ligand, saquinavir, as a canonical protease inhibitor, with their predicted BAs. The obtained results with respective binding scores and class of toxicity were presented in table 1.

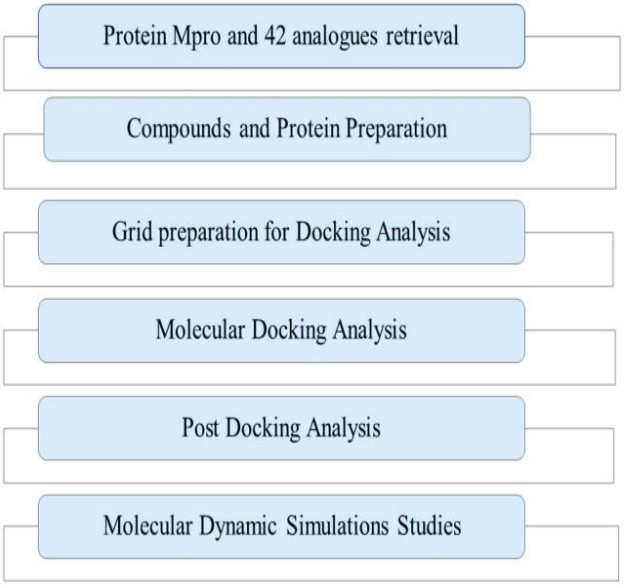

Fig. 1: Workflow of cheminformatics of SARS-CoV-2 main protease and oleanolic acid analogues applied in the current study

According to structure-based drug discovery, the modes of interaction between ligands and target protein(s) give us strong cues to screen better hits. Accordingly, the types of interaction and atoms of ligands and amino acid residues of M^{pro} have been summarized in table 2, fig. 3 and Supplementary file 1. The BAs of OA analogues showed a range of -7.7 (OA35) to -14.2 (0A11) Kcal/mol. Surprisingly, most of the OA analogues showed acceptable and reliable BAs with M^{pro} (≤-10 Kcal/mol; table 1)

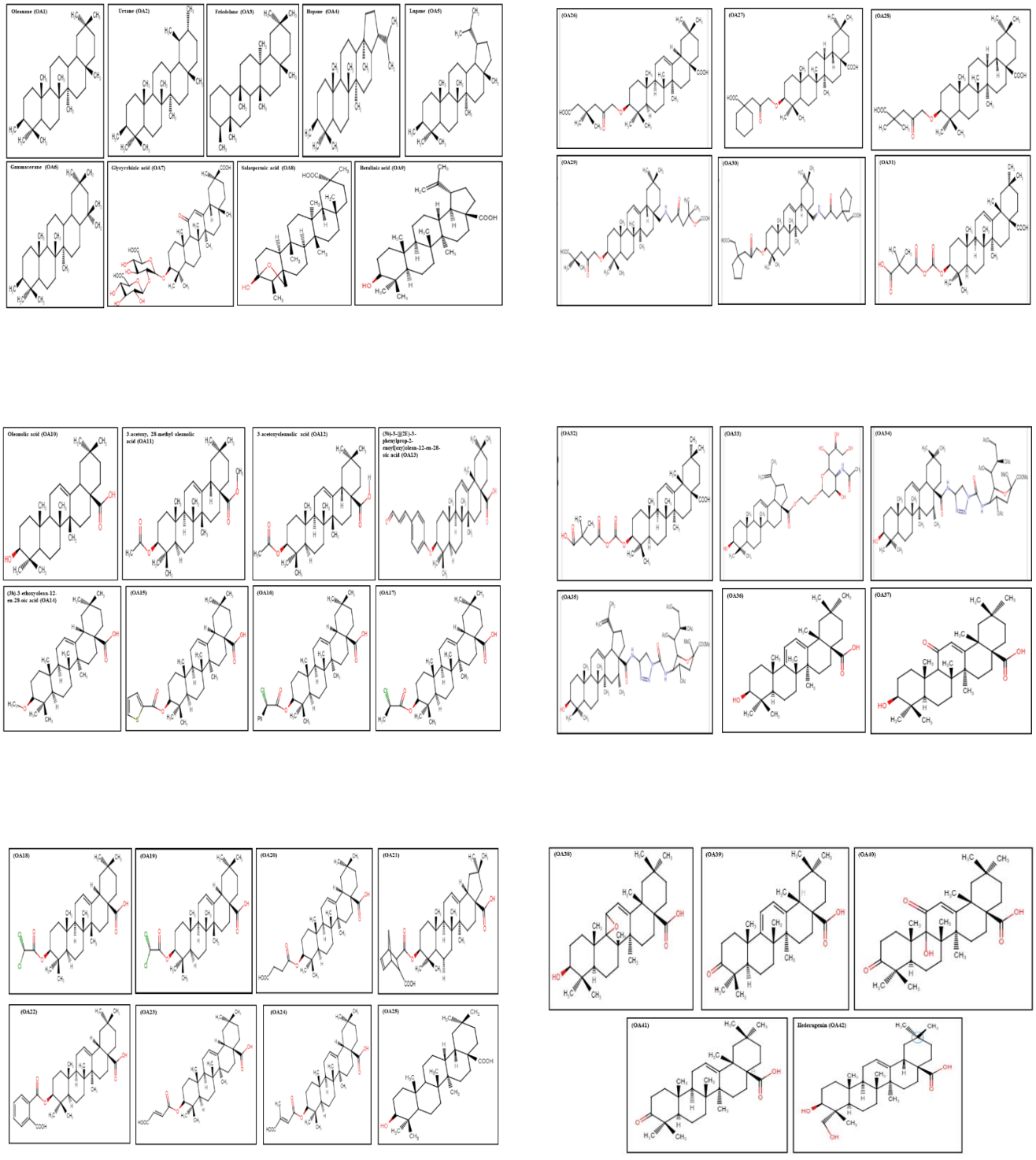

Fig. 2: The chemical structure of oleanolic acid analogues

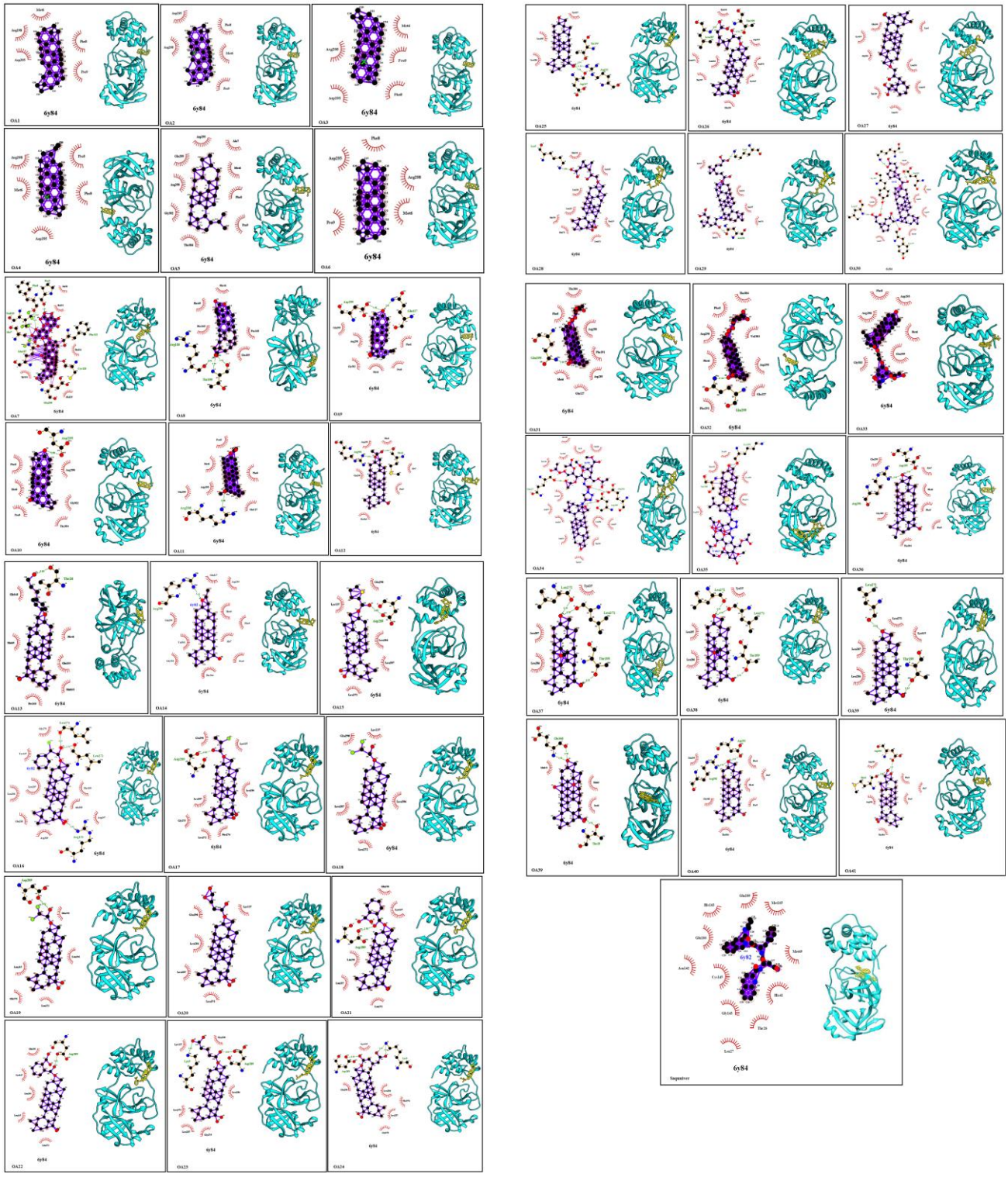

Fig. 3: The *in silico* molecular docking of oleanolic acid and its analogues (*in yellow*) against main protease of

Table 1: Molecular docking results of oleanolic acid and its analogues with protease (PDB: 6Y84) of SARS-CoV-2 and their toxicity class

Ligands No.	Canonical SMILES	Binding affinity (Kcal/mol)	RMSD/upper bound	RMSD/lower bound	Toxicity class/ Chemical feature
Oleanane-9548717 (OA1)	CC1(CCC2(CCC3(C(C2C1)CCC4C3(CCC5C4(CCCC5(C)C)C)C)C)C)C	-13.2	2.385	0.714	Low (Class I); common terpene
Ursane-9548870 (OA2)	CC1CCC2(CCC3(C(C2C1C)CCC4C3(CCC5C4(CCCC5(C)C)C)C)C)C	-13.3	5.717	0.521	Low (Class I); common terpene
Friedelane-15559345 (OA3)	CC1CCCC2C1(CCC3C2(CCC4(C3(CCC5(C4CC(CC5)(C)C)C)C)C)C)C	-13.2	5.775	0.549	Low (Class I); common terpene
Hopane-10115 (OA4)	CC(C)C1CCC2(C1CCC3(C2CCC4C3(CCC5C4(CCCC5(C)C)C)C)C)C	-11.0	32.5	29.78	Low (Class I); common terpene
Lupane ChemDraw (OA5)	CC(C)[C@@H]1CC[C@]2(C)CC[C@]3(C)C(CCC4[C@@]5(C)CC[C@H](C)C(C)(C)C5CC[C@@]34C)C12	-10.3	22.361	17.175	High (Class III); The lack of sufficient number of sulphonate or sulphamate groups
Gammacerane-9548720 (OA6)	CC1(CCCC2(C1CCC3(C2CCC4C3(CCC5C4(CCCC5(C)C)C)C)C)C)C	-13.8	5.279	0.059	High (Class III); The lack of sufficient number of sulphonate or sulphamate groups
Glycyrrhizic acid-14982 (OA7)	CC1(C2CCC3(C(C2(CCC1OC4C(C(C(C(O4)C(=O)O)O)O)OC5C(C(C(C(O5)C(=O)O)O)O)O)C)C(=O)C=C6C3(CCC7(C6CC(CC7)(C)C(=O)O)C)C)C)C	-10.8	9.905	3.332	High (Class III); The lack of sufficient number of sulphonate or sulphamate groups; Heterocyclic
Salaspermic acid–44593364 (OA8)	CC1C23CCC4C(C2CCC1(OC3)O)(CCC5(C4(CCC6(C5CC(CC6)(C)C(=O)O)C)C)C)C	-12.5	32.799	32.307	High (Class III); The lack of sufficient number of sulphonate or sulphamate groups; Heterocyclic
Betulinic acid-64971 (OA9)	CC(=C)C1CCC2(C1C3CCC4C5(CCC(C(C5CCC4(C3(CC2)C)C)(C)C)O)C)C(=O)O	-11.8	33.309	32.521	Low (Class I); common terpene
Oleanolic acid-10494 (OA10)	CC1(CCC2(CCC3(C(=CCC4C3(CCC5C4(CCC(C5(C)C)O)C)C)C2C1)C)C(=O)O)C	-12.6	6.19	0.869	Low (Class I); common terpene
3-acetoxy, 28-methyl oleanolic acid-ChemDraw (OA11)	[H][C@@]12CC(C)(C)CC[C@@]1(CC[C@]1(C)C2=CC[C@]2([H])[C@@]3(C)CC[C@H](OC(C)=O)C(C)(C)[C@]3([H])CC[C@@]12C)C(=O)OC	-14.2	5.581	1.322	Low (Class I); Open chain **;** Aliphatic with some functional groups
3-acetoxyoleanolic acid-ChemDraw (OA12)	[H]OC(=O)[C@]12CCC(C)(C)C[C@@]1([H])C1=CC[C@]3([H])[C@@]4(C)CC[C@H](OC(C)=O)C(C)(C)[C@]4([H])CC[C@@]3(C)[C@]1(C)CC2	-10.6	35.265	33.868	Low (Class I) or Class Intermediate (Class II); Readily hydrolysed to a common terpene; Open chain; Aliphatic with some functional groups

Continue

(3b)-3-{[(2E)-3-phenylprop-2-enoyl]oxy}olean-12-en-28-oic acid-ChemDraw (OA13)	[H][C@@]12CC(C)(C)CC[C@@]1(CC[C@]1(C)C2=CC[C@]2([H])[C@@]3(C)CC[C@H](OC4=CC=C(\C=C\C=O)C=C4)C(C)(C)C3([H])CC[C@@]12C)C(O)=O	-10.2	28.939	25.139	High (Class III); The lack of sufficient number of sulphonate or sulphamate groups; Aromatic; Rings with substituents; Aromatic Ring with complex substituents
(3b)-3-ethoxyolean-12-en-28-oic acid-ChemDraw (OA14)	[H][C@@]12CC(C)(C)CC[C@@]1(CC[C@]1(C)C2=CC[C@]2([H])[C@@]3(C)CC[C@H](OCC)C(C)(C)C3([H])CC[C@@]12C)C(O)=O	-10.7	33.516	31.734	High (Class III); The lack of sufficient number of sulphonate or sulphamate groups
OA15-ChemDraw	[H][C@@]12CC(C)(C)CC[C@@]1(CC[C@]1(C)C2=CC[C@]2([H])[C@@]3(C)CC[C@H](OC(=O)C4=CC=CS4)C(C)(C)[C@]3([H])CC[C@@]12C)C(O)=O	-10.2	9.099	3.069	High (Class III); The lack of sufficient number of sulphonate or sulphamate groups; Heterocyclic and Heteroaromatic with the ring bear any substituents
OA16-ChemDraw	[H][C@@]12CC(C)(C)CC[C@@]1(CC[C@]1(C)C2=CC[C@]2([H])[C@@]3(C)CC[C@H](OC(=O)C(Cl)C4=CC=CC=C4)C(C)(C)[C@]3([H])CC[C@@]12C)C(O)=O	-10.0	9.643	3.34	High (Class III); The lack of sufficient number of sulphonate or sulphamate groups; Contains elements other than C,H,O,N, divalent S
OA17-ChemDraw	[H][C@@]12CC(C)(C)CC[C@@]1(CC[C@]1(C)C2=CC[C@]2([H])[C@@]3(C)CC[C@H](OC(=O)C(C)Cl)C(C)(C)[C@]3([H])CC[C@@]12C)C(O)=O	-9.9	8.709	2.89	High (Class III); The lack of sufficient number of sulphonate or sulphamate groups; Contains elements other than C,H,O,N, divalent S
OA18-ChemDraw	[H][C@@]12CC(C)(C)CC[C@@]1(CC[C@]1(C)C2=CC[C@]2([H])[C@@]3(C)CC[C@H](OC(=O)C(Cl)Cl)C(C)(C)[C@]3([H])CC[C@@]12C)C(O)=O	-10.0	8.715	3.652	High (Class III); The lack of sufficient number of sulphonate or sulphamate groups; Contains elements other than C,H,O,N, divalent S and elements not listed in Q3 occurs only as a Na,K,Ca,Mg,N salt.
OA19-ChemDraw	[H][C@@]12CC(C)(C)CC[C@@]1(CC[C@]1(C)C2=CC[C@]2([H])[C@@]3(C)CC[C@H](OC(=O)C(Cl)Cl)C(C)(C)[C@]3([H])CC[C@@]12C)C(O)=O	-10.0	8.718	3.635	High (Class III); The lack of sufficient number of sulphonate or sulphamate groups; Contains elements other than C,H,O,N, divalent S and elements not listed in Q3 occurs only as a Na,K,Ca,Mg,N salt.
OA20-ChemDraw	[H][C@@]12CC(C)(C)CC[C@@]1(CC[C@]1(C)C2=CC[C@]2([H])[C@@]3(C)CC[C@H](OC(=O)CCC(O)=O)C(C)(C)[C@]3([H])CC[C@@]12C)C(O)=O	-9.5	9.203	2.575	Class Low (Class I); readily hydrolysed to a common terpene; Class Intermediate (Class II); Open chain; Aliphatic with some functional groups
OA21-ChemDraw	[H]C1C[C@]2(C)[C@]([H])(CC=C3[C@]4([H])CC(C)(C)C[C@@]4(CC[C@@]23C)C(O)=O)[C@@]2(C)CC[C@H](OC(=O)C3C4CC(C=C4)C3C(O)=O)C(C)(C)C12	-10.7	37.861	23.651	High (Class III); The lack of sufficient number of sulphonate or sulphamate groups; Heterocyclic

Continue…

OA22 - ChemDraw	[H][C@@]12CC(C)(C)CC[C@@]1(CC[C@]1(C)C2=CC[C@]2([H])[C@@]3(C)CC[C@H](OC(=O)C4=CC=CC=C4C(O)=O)C(C)(C)[C@]3([H])CC[C@@]12C)C(O)=O	-10.7	2.957	1.805	Class Low (Class I); Readily hydrolysed to a common terpene; Class Intermediate (Class II); Aromatic rings with substituents
OA23-ChemDraw	[H][C@@]12CC(C)(C)CC[C@@]1(CC[C@]1(C)C2=CC[C@]2([H])[C@@]3(C)CC[C@H](OC(=O)\C=C\C(O)=O)C(C)(C)[C@]3([H])CC[C@@]12C)C(O)=O	-9.9	11.862	2.52	Class Low (Class I); Class Intermediate (Class II); Open chain; Aliphatic with some functional groups
OA24-ChemDraw	[H][C@@]12CC(C)(C)CC[C@@]1(CC[C@]1(C)C2=CC[C@]2([H])[C@@]3(C)CC[C@H](OC(=O)\C=C(/C)C(O)=O)C(C)(C)[C@]3([H])CC[C@@]12C)C(O)=O	-9.1	9.676	2.288	Class Low (Class I); Readily hydrolysed to a common terpene; Class Intermediate (Class II); Aromatic rings with substituents; Open chain
OA25-ChemDraw	[H][C@]12CCC3[C@@]4(C)CC[C@H](O)C(C)(C)C4CC[C@@]3(C)[C@]1(C)CC[C@]1(CCC(C)(C)C[C@@]21[H])C(O)=O	-9.7	29.338	24.921	Low (Class I); common terpene
OA26-ChemDraw	[H][C@]12CCC3[C@@]4(C)CC[C@H](OCC(=O)CC(C)(C)CC(O)=O)C(C)(C)C4CC[C@@]3(C)[C@]1(C)CC[C@]1(CCC(C)(C)C[C@@]21[H])C(O)=O	-9.4	28.584	23.546	High (Class III); The lack of sufficient number of sulphonate or sulphamate groups
OA27-ChemDraw	[H][C@]12CCC3[C@@]4(C)CC[C@H](OCC(=O)CC5(CCCCC5)C(O)=O)C(C)(C)C4CC[C@@]3(C)[C@]1(C)CC[C@]1(CCC(C)(C)C[C@@]21[H])C(O)=O	-10.3	11.937	2.147	High (Class III); The lack of sufficient number of sulphonate or sulphamate groups
OA28-ChemDraw	[H][C@]12CCC3[C@@]4(C)CC[C@H](OCC(=O)CC(C)(C)C(O)=O)C(C)(C)C4CC[C@@]3(C)[C@]1(C)CC[C@]1(CCC(C)(C)C[C@@]21[H])C(O)=O	-9.6	1.412	1.182	High (Class III); The lack of sufficient number of sulphonate or sulphamate groups
OA29-ChemDraw	[H][C@@]12CC(C)(C)CC[C@]1(CNCC(=O)CC(C)(C)CC(O)=O)CC[C@]1(C)C2=CCC2[C@@]3(C)CC[C@H](OCC(=O)CC(C)(C)CC(O)=O)C(C)(C)C3CC[C@@]12C	-9.4	1.647	1.211	High (Class III); The lack of sufficient number of sulphonate or sulphamate groups
OA30-ChemDraw	[H][C@@]12CC(C)(C)CC[C@]1(CNCC(=O)CC1(CC(O)=O)CCCC1)CC[C@]1(C)C2=CCC2[C@@]3(C)CC[C@H](OCC(=O)CC4(CC(O)=O)CCCC4)C(C)(C)C3CC[C@@]12C	-10.4	2.181	1.735	High (Class III); The lack of sufficient number of sulphonate or sulphamate groups
OA31-ChemDraw	[H][C@@]12CC[C@]3(C)C([H])(CC=C4[C@]5(C)CC(C)(C)C[C@@]5(CC[C@@]34C)C(O)=O)[C@@]1(C)CC[C@H](OC(=O)OC(=O)CC(C)(C)C(O)=O)C2(C)C	-14.0	1.404	0.966	Class Low (Class I); Readily hydrolysed to a common terpene; Class Intermediate (Class II); Open chain; Common component of food; Aliphatic with some functional groups

Continue…

OA32-ChemDraw	[H][C@@]12CC[C@]3(C)C([H])(CC=C4[C@]5(C)CC(C)(C)C[C@@]5(CC[C@@]34C)C(O)=O)[C@@]1(C)CC[C@H](OC(=O)OC(=O)CC(C)(C)CC(O)=O)C2(C)C	-13.8	17.12	14.348	Class Low (Class I); Readily hydrolysed to a common terpene; Class Intermediate (Class II); Open chain; Common component of food; Aliphatic with some functional groups
OA33-ChemDraw	CC(=O)N[C@@H]1[C@@H](O)CC(OCCOC(=O)[C@]23CCC(C2C2=CCC4[C@@](C)(CCC5C(C)(C)[C@@H](O)CC[C@]45C)C2CC3)C(C)=C)OC1C(O)C(O)CO	-12.3	13.43	10.843	High (Class III); The lack of sufficient number of sulphonate or sulphamate groups; Heterocyclic with ring with complex
OA34-ChemDraw	COC(=O)C1(CC(OC(C)=O)C(NC(=O)N2CC(NC(=O)[C@]34CCC(C)(C)CC3C3=CCC5[C@@]6(C)CC[C@H](O)C(C)(C)C6CC[C@@]5(C)[C@]3(C)C[C@H]4C)N=N2)C(O1)C(OC(C)=O)[C@@H](COC(C)=O)OC(C)=O)OC	-8.6	15.278	5.867	High (Class III); The lack of sufficient number of sulphonate or sulphamate groups; Heterocyclic ring with complex substituents
OA35-ChemDraw	COC(=O)C1(CC(OC(C)=O)C(NC(=O)N2CC(NC(=O)[C@]34CC[C@H](C3C3=CCC5[C@@]6(C)CC[C@H](O)C(C)(C)C6CC[C@@]5(C)[C@]3(C)C[C@H]4C)C(C)=C)N=N2)C(O1)C(OC(C)=O)[C@@H](COC(C)=O)OC(C)=O)OC	-7.7	28.046	20.856	High (Class III); The lack of sufficient number of sulphonate or sulphamate groups; Heterocyclic ring with complex substituents
OA36-ChemDraw	[H][C@@]12CC[C@]3(C)C(=CC=C4[C@@]3(C)CC[C@]3(CCC(C)(C)C[C@@]43C)C(O)=O)[C@@]1(C)CC[C@H](O)C2(C)C	-10.6	26.352	22.158	High (Class III); The lack of sufficient number of sulphonate or sulphamate groups
OA37-ChemDraw	[H][C@@]12CC[C@@]3(C)[C@]4(C)CC[C@]5(CC[C@H](C)C[C@@]5(C)C4=CC(=O)C3(O)[C@@]1(C)CC[C@H](O)C2(C)C)C(O)=O	-9.8	32.38	27.083	High (Class III); The lack of sufficient number of sulphonate or sulphamate groups
OA38-ChemDraw	[H][C@@]12CC[C@]3(C)C4(OC4C=C4[C@@]3(C)CC[C@]3(CCC(C)(C)C[C@@]43C)C(O)=O)[C@@]1(C)CC[C@H](O)C2(C)C	-10.7	26.122	22.013	High (Class III); Heterocyclic
OA39-ChemDraw	[H][C@@]12CC[C@]3(C)C(=CC=C4[C@@]3(C)CC[C@]3(CCC(C)(C)C[C@@]43C)C(O)=O)[C@@]1(C)CCC(=O)C2(C)C	-10.7	26.015	21.892	High (Class III); The lack of sufficient number of sulphonate or sulphamate groups
OA40-ChemDraw	[H][C@@]12CC[C@@]3(C)[C@]4(C)CC[C@]5(CCC(C)(C)C[C@@]5(C)C4=CC(=O)C3(O)[C@@]1(C)CCC(=O)C2(C)C)C(O)=O	-10.6	7.718	1.402	High (Class III); The lack of sufficient number of sulphonate or sulphamate groups
OA41-ChemDraw	[H][C@@]12CC[C@]3(C)[C@]([H])(CC=C4[C@@]3(C)CC[C@]3(CCC(C)(C)C[C@@]43C)C(O)=O)[C@@]1(C)CCC(=O)C2(C)C	-10.8	26.326	22.248	High (Class III); The lack of sufficient number of sulphonate or sulphamate groups

Continue…

Hederagenin (OA42)-ChemDraw	[H][C@@]12CC(C)(C)CC[C@@]1(CC[C@]1(C)C2=CC[C@]2([H])[C@@]3(C)CC[C@H](O)[C@@](C)(CO)[C@]3([H])CC[C@@]12C)C(O)=O	-10.2	25.998	21.54	Low (Class I); common terpene
Saquinavir-DrugBank	CC(C)(C)NC(=O)C1CC2CCCCC2CN1CC(C(CC3=CC=CC=C3)NC(=O)C(CC(=O)N)NC(=O)C4=NC5=CC=CC=C5C=C4)O	-8.1	1.433	1.202	High (Class III); The lack of sufficient number of sulphonate or sulphamate groups; Heterocyclic ring with complex substituents

RMSD: root mean-square deviation is the measure of the average distance between the atoms. See [1] for more details.

Table 2: The chemical dissection of the interactions of oleanalic acid analogues and protease (PDB: 6Y84) of SARS-CoV-2

Ligands No.	Hydrogen bond	Hydrophobic interaction	Interacted atoms of ligands	No. in Fig. 2
Oleanane (OA1)	ND	V303, R298, F8, D295, Q127, A7, M6, and P9	-	1
Ursane (OA2)	ND	V303, P9, M6, A7, Q127, F8, D295, and R298	-	2
Friedelan (OA3)	ND	D298, Q127, A7, F8, P9, V303, M6, and D295	-	3
Hopane (OA4)	ND	R298, F8, P9, A7, V303, M6, D295 and Q127	-	4
Lupine (OA5)	ND	P9, A7, Met6, R298, Q127, Asp295, F8, Q299, V303 G302, and T304	-	5
Gammacerane (OA6)	ND	P9, A7, Q127, F8, D295, M6, R298, and V303	-	6
Glycyrrhizic acid (OA7)	P9 and double with F8	T111, A129, N151, I152, S10, V13, Y126, and M6	O_{15}, O_{16}, O_8 with P9 and F8 and O_8, O_{10} with V125 and O_{10}, O_{11}, C_{37} with A7, and O_2, C_{19}, C_1, C_2, C_{19}, C_{13} with Q27 and C_{23}, C_{28} with E290, and C_{20}, C_{12} with C128 and C_6, C_7, C_{25} with F112	7
Salaspermic acid (OA8)	R188 and T190	M165, M49, His41, E166, P168, Q189, Q192 and L167	O_3 with R188 and O_3, O_2 with T190	8
Betulinic acid (OA9)	Q127and D295	A7, P9, F8, R298, M6, Q299, G302, and V303	O_3 with Q127 and D295	9
Oleanolic acid (OA10)	D295	P9, M6, F8, A7, R298, Q127, V303, G302 and T304	O_3	10
3-acetoxy, 28-methyloleanolic acid (OA11)	R298	Q127, D295, M6, V303, P9, Q299 and F8	O_3	11
3-acetoxyoleanolic acid (OA12)	M6 and R298	P9, F8, A7, Q127, Q299, D295, V303 and T304	O_2 with M6 and O_1 with R298	12
(3b)-3-{[(2E)-3-phenylprop-2-enoyl]oxy}olean-12-en-28-oic acid (OA13)	T26	T190, Met165, Q192, Met49, His41, G143, G189, R188, E166 and P168	O_2	13
(3b)-3-ethoxyolean-12-en-28-oic acid (OA14)	R298	T304, P9, A7, F8, M6, D295, Q127, Q299, V303, and 302	O_1	14
OA15	D289	272, Y239, Y237, Thr199, R131, D197, E290, K137, L286 and L287	O_2	15
OA16	D131, L272 and L271	D197, Ala285, T199, G275, Y237, L287, L287, E288 and D289	O_2 with L272, and l271 and O_4 with D131	16
OA17	D289	L272, Tyr237, Y239, Thr199, D197, R131, E290, Y137, L286, M276, G275 and L271	O_2	17

Continue…

8OA18	ND	L272, Y237, Y239, Thr199, D197, K137, E290, Arg131, L286, L287 and Leu271	-	18
OA19	D289	L271, L272, Y239, Tyr237, T199, D197, R131, Lys137, E290, L286, L287 and G275	O_2	19
OA20	ND	Y237, Y239, T199, Asp197, R131, E290, K137, L286, L287, L271 and L272	-	20
OA21	D289	L272, Y239, Y237, T199, R131, D197, K137, E290, E288, L286, L287 and L271	O_2	21
OA22	D289	L271, Tyr237, Y239, L272, T199, Asp197, K137, E288 E290, Arg131, Leu286 and L287	O_2	22
OA23	D289 and K5	Y239, TY237, L272, Thr199, Asp197, R131, E290, K137, L286, G275, L287 and L271	O_2 with D289 and O_4 with K5	23
OA24	K5 and D289	L271, L272, Y137, Y239, T199, Arg131, D197, E290, K137, L286, M276, L287 and G275	O_2 with D289 and O_2, O_4 with K5	24
OA25	T199, R131, D197	Y237, L272, L287, L286, D289, and T198	O_1	25
OA26	L287 and T199	K5, K137, E290, R131, D197, Y137, Y239, L272, L286 and G288	O_3 with L287 and O_4 with T199	26
OA27	ND	L272, Leu287, 286, E288, K5, Q127, C128, Tyr126, E290, K137, D289, R131, Y239 and T199	-	27
OA28	K5	L271, L272, Y237, T199, D197, Lys137, R131, E290, E288, L286, M276, L287 and G275	O_2	28
OA29	K5 and N238	L272, L271, L287, L286, E290, C128, K137, Q127, T199, D197 and Y237	O_5 with K5 and O_3 with N238	29
OA30	Y237, L287, Y239, K5 and E288	T99, D197, D289, R131, E290, L286 and L272	O_3 with Y237 and O_1 with L287, and O_2 with Y239 and O_5 with K5 and O_5 with E288	30
OA31	Q299	Q127, D295, M6, I152, T304, F8, P9, V303, R298 and F291	O_8	31
OA32	Q299	D295, M6, F291, Q127, R298, P9, I152, F8, T304 and V303	O_8	32
OA33	ND	Q299, M6, D295, D127, F8, R298, V303 and G302	-	33
OA34	Q127, E290 and D289	T199, L287, L286, E288, K5, G138, C128, Y126, K137, D197, R131, L272 and Y237	O_8, O_{16} with E290 and N_5 with D289	34
OA35	K100 and S158	F103, cys156, P99 F159 and R105	O_2, C_3 with K100 and C_3, C_{19} with S158	35
OA36	D295 and R298	T304, P9, V303, M6, A7, F8, Q290 and G302	O_3	36

Continue…

OA37	T25, E189 and N142	Y45, S46, M49, Q189, M165, C145 (Cys145), T24 and T26	O5 with E189 and O4 with N142 and O2 with T25	37
OA38	L272, L271 and T199	D289, D197, Y198, Y237, Leu287 and Leu286	O_4 with L272, L271 and O_2 with T199	38
OA39	L271 and T199	D197, T198, L287, Tyr237, L272 and L286	O_3 with L271 and O_2 with T199	39
OA40	E166 and T25	T45, S46, M149, Q189, M165, N142, Cys145, Thr26 and Thr24	O_5 with E166 and O_2 T25	40
OA41	Q299 and D295	T45, S46, M149, Q189, M145, N142, Cys145, Thr26 and Thr24	O_5 with Q299 and O_2 with D295	41
Hederagenin (OA42)	D295 and M6	F8, Pro9, Q127, A7, R298, Q299, V303, Gly302 and T304	O_2 with D295 and O_1 with M6	42
Saquinavir	ND	T26, His41, M49, M165, Q189, H163, E166, N142, C145 Cys145) and G143	ND	saquinavir

Note: ND: not detected

ADME analysis

The classes of toxicity which OA analogues belonged showed considerable variation. In this context, analogues 16, 6 and 15 were belonged to the low (Class I), low (Class I) or intermediate (Class II) and highly toxic (Class III), respectively. Among low (Class I) toxic compounds, the strongest BA was reported for OA11 (-14.2) and OA31 (-14.0 Kcal/mol) and these two ligands were submitted for MD (*vide infra*). In this context, the safest compound was OA11 since OA31 was much closer to intermediate (Class II) toxic compounds. All results of ADME are presented in Supplementary file 2.

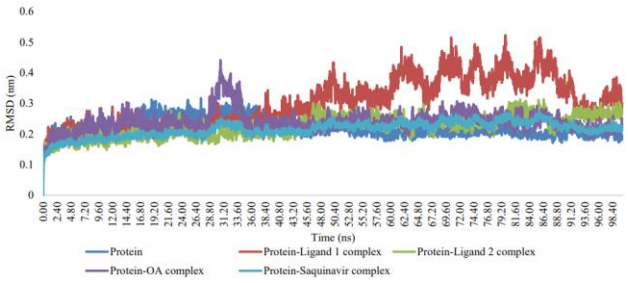

Fig. 4: RMSDs of SARS-CoV-2 M^{pro} in the ligand-free form and in the presence of oleanolic acid, ligand I, ligand II and saquinavir.

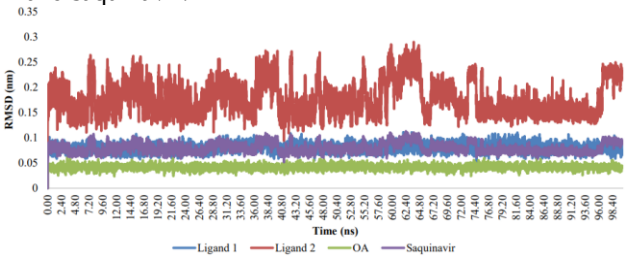

Fig. 5: RMSDs of oleanolic acid, ligand I and ligand II and saquinavir inside the active site of SARS CoV-2 M^{pro} Over the course of 100 ns-long MD simulation. OA showed the lowest average RMSD (~0.05 nm) and the most stable binding inside the active site of M^{pro}, while ligand 2 was the least stable ligand with an average RMSD of 0.21 nm over the simulation time. The RMSD profiles of both ligand 1 and saquinavir were convergent with an average of ~ 0.09 nm.

Molecular docking and trajectories analysis

Molecular docking offers practical binding structures while MD simulation enables us to understand structure and dynamics in detail for further investigation of the binding modes of ligands and explanation. In this study, GROMACS analysis tools were employed to analyze the trajectories in terms of root mean square deviation (RMSD), root mean square fluctuation (RMSF), radius of gyration (R_g), H-bond frequency, and the secondary structure.

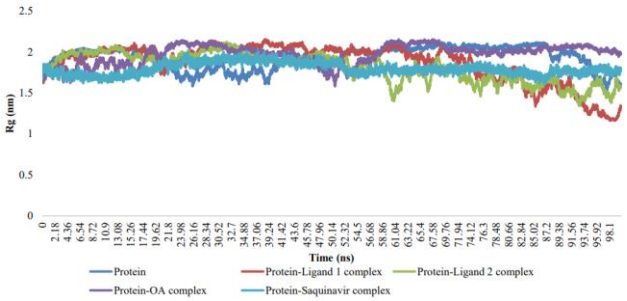

Fig. 6: Time dependence of the R_g of the protein during the simulation for free and bound SARS-CoV-2 main protease

To confirm the stability of simulations, the RMSD of protein in the absence and presence of OA, ligand I, ligand II and saquinavir were analyzed during 100 ns simulation time. The result highlighted that these compounds remain in a stable binding position with low RMSD fluctuations which confirms the feasibility of binding poses predicted by AutoDock. The mean RMSD values for protein, protein in complex with the OA, ligand I, ligand II and saquinavir were 0.267 nm, 0.238 nm,

0.215 nm and 0.225 nm, respectively (fig. 4,5). The highest value of mean RMSD for SARS-CoV-2 M^{pro} represents the formation of stable complexes of this protein with these compounds. Moreover, the lowest value of mean RMSD for protein in complex with ligand I signifies the formation of most stable complex of protein with this compound.

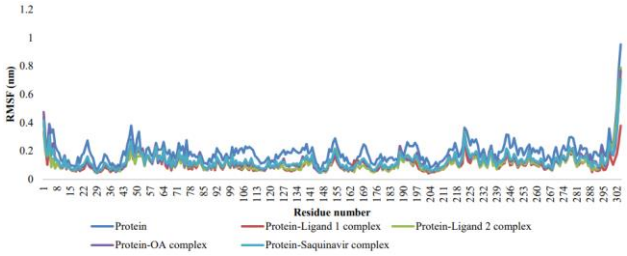

Fig. 7: RMSF of residues of protein from their time averaged positions during last 20 ns for free and bound SARS-CoV-2 main protease

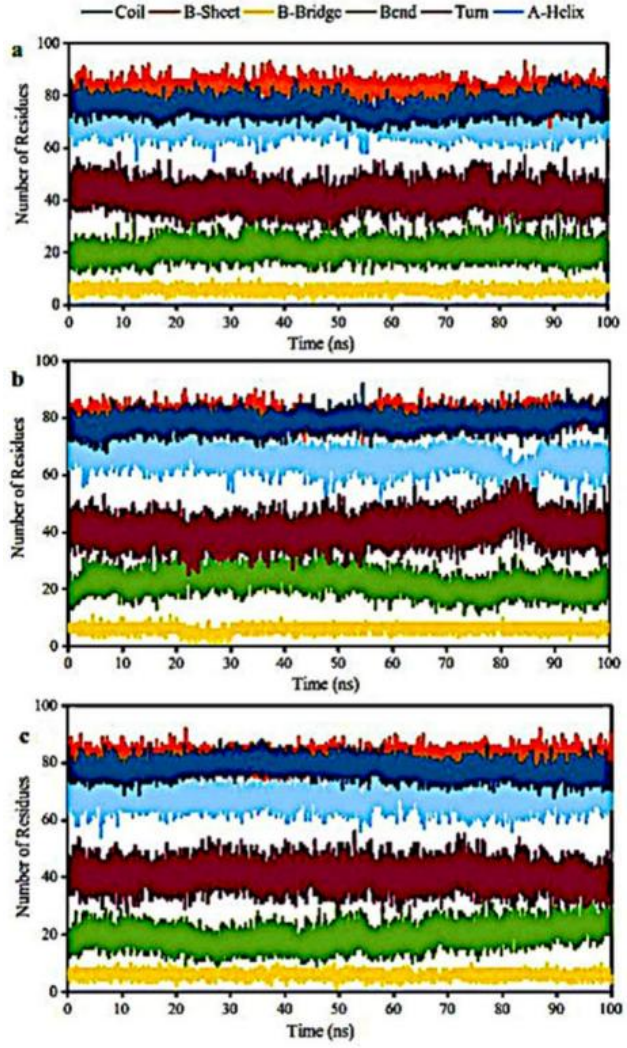

Fig. 8: Variation of the secondary structure versus time for the protein in the presence of a) Oleanolic acid, b) ligand I and c) ligand II

The compactness of protein structure during MD simulation time was assessed by analysis of the radius of gyration (R_g). As illustrated in fig. 6, the R_g of SARS-CoV-2 M^{pro} decreased with binding of all three compounds implying a more compact structure of this protein after simulations.

The RMSF analysis of SARS-CoV-2 M^{pro} in the absence and presence of OA, ligand I and ligand II can be used as a reference value to estimate the flexibility of the residues (fig. 7). The results produced by RMSF analysis of protein during the last 20 ns indicated that main fluctuations (> 0.2 nm) correspond to residues belonging to the mobile loops of protein which are far from the ligand binding site. In contrast, residues which were found to interact with these compounds in the binding site of SARS-CoV-2 M^{pro} are among the most stable residues of this protein (RMSF < 0.10 nm).

The secondary structure of the protein was calculated with the DSSP code of GROMACS. Fig.**8 shows** the α-helix, β-Sheet and other secondary structures of the protein in three simulations. As demonstrated in this fig. 8, main secondary structures of SARS-CoV-2 M^{pro} maintain fair stability during 100 ns MD simulations. Therefore, the principal conformational change of protein proposed during binding of the OA, ligand I and ligand II is a simple motion.

The total number of hydrogen bonds between SARS-CoV-2 M^{pro} and OA, ligand I and ligand II were calculated using the g_hbond function of GROMACS which, the geometry standard of H-bonds was 0.35 nm for H-accepter distance and 3.0 nm for the donor-H-acceptor angle. The analysis of H-bonds showed that ligand I has more H-bonds compared to those of OA and ligand II which suggests the formation of most stable complex of protein with this compound (fig. 9).

DISCUSSION

Many PTs show numerous pharmacological activities and some are even marketed as therapeutic agents or dietary supplements [46]. Structurally, PTs have four six membered rings characterized as A, B, C, D plus ring E being five-membered or six-membered structures. Based on the carbon skeleton, they are allocated into six common subgroups: oleanane, lupane, ursane, friedelane, hopane and gammacerane. In this regard, PTs are a large class of secondary plant metabolites constructed by isoprene (2-methylbutadiene; C5H8) units [16, 47]

Oleanane (OA1) is a PT and with its congeners possess anti-viral activity for influenza virus, hepatitis virus, HIV, and porcine epidemic diarrhea virus [1, 48-51]. Moreover, OA1 is known as a modulator of influenza hemagglutinin (HA).

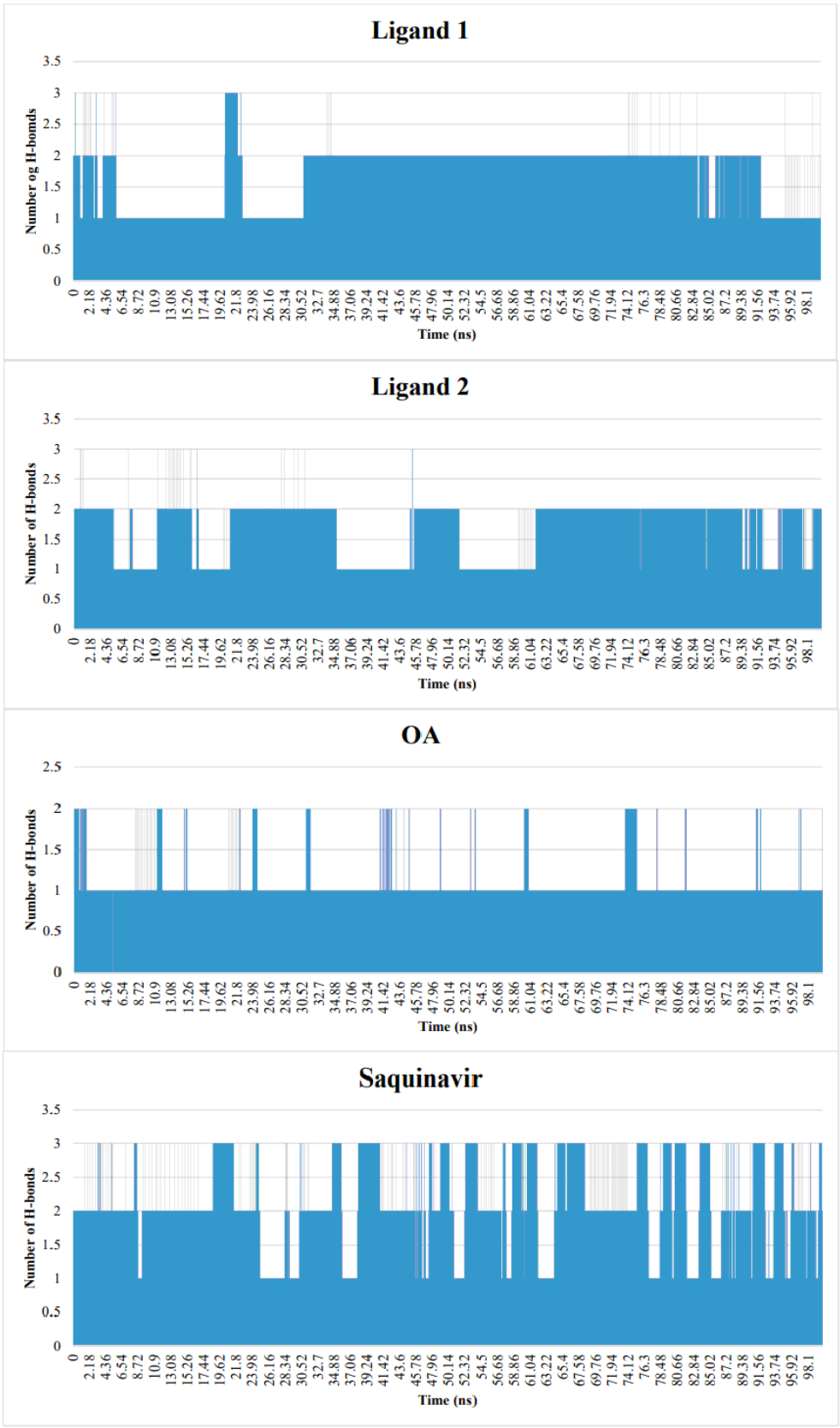

Fig. 9: Time dependence of total number of hydrogen bonds between protein and a) Oleanolic acid (OA), b) ligand I and c) ligand II

The glycosylated OA intensified the HA inhibitory activity of OA with no overt cytotoxicity upon Madin-Darby canine kidney cells [50, 52]. Ursane (OA2) belongs to PTs and it has anti-inflammatory, anti-microbial, cytotoxic, hepatoprotective and anti-tumor activities [53-55]. Friedelane (OA3) is a natural PT alkane belongs to friedelane triterpenoids [56]. Its skeleton stands behind its efficacy gives rise to be considered as lead molecules for designing anti-coronaviral agents [52]. Another study reported that 3β-friedelanol has more anti-viral activity than that of actinomycin D because of the presence of friedelane skeleton as a scaffold for combinatorial designing of new generation of anti-viral agents for human coronavirus 229E [57]. Another study showed that leaf ethanolic extract of *Euphorbia neriifolia* L. from Taiwan contained one flavonoid and 22 triterpenoids [57]. In this regard, the strongest inhibitor of human coronavirus (229E strain) was 3β-friedelanol. As strongly supported by evidence, friedelane triterpenoids possess anti-HIV, anti-microbial, and anti-neoplastic potentials [56]. In this study, OA1, OA2 and OA3 provided equal amount of BA (-13 Kcal/mol) with low toxicity (table 1).

Hopane (OA4) is a triterpene that forms the central nucleus of hopanoids. In this category, hydroxyhopanone has been initially characterized [58]. New hopane-type triterpenoids exhibited noteworthy antifungal activity [59]. In this study, OA4 showed BA of -11.0 Kcal/mol with low toxicity (table 1).

Lupane (OA5) with BA of -10.3 Kcal/mol (table 1) is a lupane-type saponin presenting weak cytotoxic activity for Cellosaurus HSC-2 cells [60]. In this line, betulinic and betulin acid and their analogues showed anti-HIV-1 activity at *in vitro* level [61]. Gammacerane (OA6) with BA of -13.8 Kcal/mol (table 1) is considered an irregular biodegradation-resistant C30 PT [62]. Glycyrrhizic acid (OA7; GA) is an oleanane-type triterpenoid with BA of -10.8 Kcal/mol (table 1) which reportedly showed anti-HSV-1 (Herpes simplex virus 1) activity [63] and attenuated inflammation in HSV [64]. The GA is also derived from β-amyrin type found in liquorice (*Glycyrrhiza glabra*). Accordingly, GA inhibits different viruses including HIV and hepatitis B virus (HBV) [16, 65]. Moreover, PTs such as glycyrrhizin and 18β-glycyrrhetinic acid are considered as a source of flavoring agent and sweetener [66]. In this line, α and β stereoisomers of GA express anti-tumor and anti-inflammatory activities [67]. The reliable BA of GA with Coronavirus main proteinase (3CLpro) was reported by our team for the first time [22] however, a seminal study using network pharmacology showed that GA ameliorates cytokine storm response to SARS-CoV-2 [68]. In this essence, lupane, gammacerane and GA belong to high toxicity class III (table 1).

Salaspermic acid (OA8) with BA of -12.5 Kcal/mol (table 1) is toxic oleanane-type triterpene derivative which can inhibit the HIV replication in H9 lymphocytes [16, 69]. Betulinic acid (OA9; Bet A) is a PT isolated initially from the birch trees [66, 70, 71]. Bet A can express a wide range of anticancer activities for neuroblastoma, melanoma, estrogen receptor negative breast cancer, cervical cancer, colon cancer, ovarian cancer, prostate cancer, and lung cancer [72, 73]. Additionally, Bet A can also serve strong antiviral, anti-HIV, antibacterial, anti-inflammatory, anthelmintic, anticancer, and antimalarial activities [74]. The protease of SARS-CoV-2 (PDB ID: 6LU7) is a major player in the viral replication. Results of molecular docking with 6LU7 and its similar structures showed that Bet (A8) had the strongest BA (-11.53 Kcal/mol) among all derivatives [74]. In the present study, Bet A interacted with M^{pro} with BA of -11.8 Kcal/mol.

Oleanolic acid (OA10; OA) is one of the most common PTs found in various herbal sources especially prevalent in plants belonging to Oleaceae (olive) family [75, 76]. Among all species of Oleaceae family, olive (*Olea europaea* L.) [77, 78] is still the main source of commercial OA [79]. In these plants, OA is often distributed in epicuticular waxes where it acts as a barrier against water loss and pathogens [80]. The OA content is much higher in fruit "skin" rather than pulp [78, 81]. In addition to olives, Mediterranean diet is enriched with OA due to the inclusion of legumes contain OA (0.251-2.591 µg/g fresh weight) [82]. A large amount of OA is also present in *Ziziphus jujube* Mill. which is a routinely consumed fruit in China Southern and Asia [83]. Oleanolic acid and its derivatives have antioxidative, antiviral, anti-inflammatory and anti-diabetic effects [84]. The hepato-protective effects of OA make it a suitable over-the-counter oral drug to treat hepatic diseases such as viral hepatitis in China [76, 85, 86]. In this line, OA upturns nuclear Nrf2, thereby leading to the induction of Nrf2-dependent genes playing a role in hepato-protection [85, 87]. Moreover, the anticancer effects of OA were reported in the malignancies including hepatocellular cancer [88], breast cancer [51], and lung cancer [89]. The OA-mediated inhibition of tumor growth is widely demonstrated in diverse models. For instance, OA is reported to inhibit the growth of transplanted tumor in mice and proliferation of hepatocellular carcinoma cells (HepG2). The anti-tumor activity of OA is undertaken through upregulating tumor protein (p53), cyclooxygenase-2 mediated activation of mitochondrial apoptotic pathway. Furthermore, OA like acyclovir showed an anti-HSV effect during replication resulting in reduced viral load confirmed by polymerase chain reaction [90]. In the present study, OA interacted with M^{pro} with BA of -12.6 Kcal/mol. In this line, other study [91] reported that ursolic acid, carvacrol and OA passed Lipinski's rule of five with reliable BAs for SARS-CoV-2 M^{pro}.

3-acetoxy, 28-methyloleanolic acid (OA11) and 3-acetoxyoleanolic acid (OA12) are semisynthetic derivatives of OA which possess anti-inflammatory activity and showed erythrocyte membrane-stabilizing properties [92]. The OA11, presented as ligand I in this study (*vide infra*), showed the strongest BA (-14.2 Kcal/mol) with M^{pro}; however, there exist no experimental confirmation supporting its anti-protease or anti-viral activities and further investigations are acknowledged. The interaction between OA12 and M^{pro} displayed BA of -10.6 Kcal/mol and OA9-OA12 were low (class I) toxic compounds (table 1). The antiviral and antithrombotic activities of OA13 and OA14 have been reported [1]. Although these two molecules showed good BAs with M^{pro}, they were high toxic compounds (table 1). The OA15 to OA30 and OA34 to OA42 showed BAs more than -11.0 Kcal/mol and/or they were toxic compounds; therefore, their anti-viral activities have not been discussed and we would like to seize the readers' attention to a seminal review [1] for more information.

The M^{pro} (PDB ID: 6Y84) contains three domain I, II, and III containing 8-101, 102-184 and 201-306 amino acid residues, respectively. Domain I and II mainly consists of β-barrels while domain III mainly consists of α-helix strands. The substrate-binding active site is a cleft between domain I and II which consists of cysteine–histidine catalytic dyad H-41 and C-145 as two catalytic residues. In the present study, OA8, OA13 and saquinavir interacted with M-165, E-166, M-49 and H-41 of M^{pro} among others while OA37 and OA40 interacted with C-145 in catalytic dyad and M-165 residue in active site (table 2; fig. 3; Supplementary file 1). The OA37 also interacted hydrophobically with M-49 of M^{pro} whereas OA-40 employed hydrogen bonds to interact with M^{pro}. The majority of binders or inhibitors of M^{pro} interact at His-41, His-163, His-164, Cys-145, Glu-166, Met-49 and Met-165 residues via aromatic π-π stacking and hydrogen bonds [93]. To sum up, OA8, OA13, OA37, OA40 and saquinavir were identified as potential hits employing different interactions with M^{pro} (table 2; fig. 3; Supplementary file 1). In addition, OA11 showed strong BA for M^{pro} through the interaction with residues R298 using hydrogen bond and an array of similar amino acid residues in comparison with those of OA10 which interacted through hydrophobic interactions. The OA31 in the second order of BA for M^{pro} also employed Q299 residue in hydrogen bond and a set of amino acids to interact hydrophobically.

We could not present the molecular interactions of OA analogues with all possible targets of SARS-CoV-2, more investigations are acknowledged to dissect this issue. Based on the structures of PTs, the possibility of chemical promiscuity should be pursued in future studies. Herein, we placed our focus on saquinavir as a counter-reference to compare its *in silico* binding to 3-chymotrypsin (6Y84 PDB) compared to OA analogues links to untangle which phytocompounds could participate in anti-coronoviral effects (table 1). M^{pro} is considered one of the key enzymes responsible for the replication and transcription of the coronavirus. Therefore, this study was aimed to explore the activity of these compounds as potent anti-SARS-CoV-2 molecules by employing simulation studies [94].

CONCLUSIONS

In current health crisis caused by COVID-19, the identification of novel OA derivatives as potent lead-like or drug-like compounds should be taken into consideration as a novel opportunity. All 42 analogues were subjected to molecular docking against M^{pro} of SARS-CoV-2. Findings revealed that all compounds showed BAs ranging from -7.7 to -14.2 Kcal/mol having stable interaction with M^{pro}. However, MD simulation identified OA, ligand I, and ligand II as recommended lead-like compounds. Moreover, the identified compounds need to be validated through future studies to more confirmation of their possible anti-SARS-CoV-2 efficacies. To sum up, OA8, OA13, OA37 and OA40 interacted with catalytic dyad and major amino acid residues of active sites of M^{pro} and these striking features make them suitable candidate for future development of antiviral anti-proteases.

DECLARATION OF COMPETING INTEREST

It is hereby declared that author has neither financial nor non-financial interests to disclose.

REFERENCES

1. Khwaza, V., O.O. Oyedeji, and B.A. Aderibigbe, *Antiviral activities of oleanolic acid and its analogues.* Molecules, 2018. **23**(9): p. 2300.
2. Bakhtiyari, E., I. Karimi, and L.J. Mohammed, *Psychobiotics and Thanatophobia: A Psychoneuroimmunological Insight into Microbe-Mind Modification.*
3. Brief, T.A., *Rapid increase of a SARS-CoV-2 variant with multiple spike protein mutations observed in the United Kingdom.* Epidemiology, 2020. **7**: p. 1-3.
4. Nikhra, V., *Evolving patterns in COVID-19: the virus, its variants and infectivity-cum-virulence.* Biomed J Sci Tech Res, 2021. **33**(2).
5. Mecenas, P., et al., *Effects of temperature and humidity on the spread of COVID-19: A systematic review.* PLoS one, 2020. **15**(9): p. e0238339.
6. Van Asten, L., et al., *Excess deaths during influenza and coronavirus disease and infection-fatality rate for severe acute respiratory*

syndrome coronavirus 2, the Netherlands. Emerging infectious diseases, 2021. **27**(2): p. 411.
7. Aghbash, P.S., et al., *Viral coinfections in COVID-19.* Journal of Medical Virology, 2021. **93**(9): p. 5310-5322.
8. Gianfredi, V., et al., *Challenges and opportunities of mass vaccination centers in COVID-19 times: a rapid review of literature.* Vaccines, 2021. **9**(6): p. 574.
9. Voigt, K., E. Nahimana, and A. Rosenthal, *Flashing red lights: the global implications of COVID-19 vaccination passports.* BMJ Global Health, 2021. **6**(5): p. e006209.
10. Redmond, S.N., et al., *Severe acute respiratory syndrome coronavirus 2 (SARS-CoV-2) infection in vaccinated and unvaccinated healthcare personnel in a Veterans' Affairs healthcare system.* Infection Control & Hospital Epidemiology, 2022. **43**(9): p. 1300-1301.
11. Villamagna, A.H., et al., *The need for antiviral drugs for pandemic coronaviruses from a global health perspective.* Frontiers in Medicine, 2020: p. 998.
12. Ahmed, H.M., *Ethnopharmacobotanical study on the medicinal plants used by herbalists in Sulaymaniyah Province, Kurdistan, Iraq.* Journal of ethnobiology and ethnomedicine, 2016. **12**(1): p. 1-17.
13. Ali, A.M. and H. Kunugi, *Propolis, bee honey, and their components protect against coronavirus disease 2019 (Covid-19): A review of in silico, in vitro, and clinical studies.* Molecules, 2021. **26**(5): p. 1232.
14. Khanal, P., et al., *Withanolides from Withania somnifera as an immunity booster and their therapeutic options against COVID-19.* Journal of Biomolecular Structure and Dynamics, 2022. **40**(12): p. 5295-5308.
15. Fabbri, N., et al., *Risks of COVID-19 transmission in blood and serum during surgery A prospective cross-sectional study from a single dedicated COVID-19 center.* Ann Ital Chir, 2020. **91**: p. 235-238.
16. Xiao, S., et al., *Recent progress in the antiviral activity and mechanism study of pentacyclic triterpenoids and their derivatives.* Medicinal research reviews, 2018. **38**(3): p. 951-976.
17. Acton, Q.A., *Immune System Diseases: New Insights for the Healthcare Professional: 2013 Edition*. 2013: ScholarlyEditions.
18. Chepkwony, P.K., M. Medina, and M. Medina, *Compounds and compositions for treating infection*. 2012, Google Patents.
19. Hung, T.-C., et al., *Lead screening for CXCR4 of the human HIV infection receptor inhibited by traditional Chinese medicine.* BioMed Research International, 2014. **2014**.
20. Shi, H., et al., *Baicalin from Scutellaria baicalensis blocks respiratory syncytial virus (RSV) infection and reduces inflammatory cell infiltration and lung injury in mice.* Scientific reports, 2016. **6**(1): p. 1-12.
21. Wu, T.-S., *Herbal pharmaceutical composition for treatment of HIV/AIDS patients*. 2004, Google Patents.
22. Mohammed, H.N.M., Layth Jasim; Karimi, Isaac; & Suvitha, A, *A Computational Effort to Deciphering Putative COVID-19 3C-like Protease Binders in the Selected Recipes of Kurdish Ethnomedicine: An Approach to Find an Antiviral Functional Tea*, in *Functional Foods and Viral Diseases*, P. Danik M Martirosyan, Editor. 2020, Food Science Publisher.
23. AbrahamDogo, G., et al., *Molecular docking analyses of phytochemicals obtained from African antiviral herbal plants exhibit inhibitory activity against therapeutic targets of SARS-CoV-2.* 2020.
24. Matondo, A., et al., *Oleanolic acid, ursolic acid and apigenin from Ocimum basilicum as potential inhibitors of the SARS-CoV-2 main protease: A molecular docking study.* Int J Pathog Res, 2021. **6**(2): p. 1-16.
25. Pawełczyk, A. and L. Zaprutko, *Anti-COVID drugs: repurposing existing drugs or search for new complex entities, strategies and perspectives.* Future Medicinal Chemistry, 2020. **12**(19): p. 1743-1757.
26. Dallakyan, S. and A.J. Olson, *Small-molecule library screening by docking with PyRx*, in *Chemical biology*. 2015, Springer. p. 243-250.
27. Thomsen, R. and M.H. Christensen, *MolDock: a new technique for high-accuracy molecular docking.* Journal of medicinal chemistry, 2006. **49**(11): p. 3315-3321.
28. Laskowski, R.A. and M.B. Swindells, *LigPlot+: multiple ligand–protein interaction diagrams for drug discovery*. 2011, ACS Publications.
29. Lipinski, C.A., et al., *Experimental and computational approaches to estimate solubility and permeability in drug discovery and development settings.* Advanced drug delivery reviews, 1997. **23**(1-3): p. 3-25.
30. Abdulhussein, J.M., et al., *The phytobiotic potential of hydro-alcoholic extract of Allium porrum against Bacillus cereus: A computational sight into PlcR protein as a putative target.* Biocatalysis and Agricultural Biotechnology, 2021. **35**: p. 102062.
31. Cramer, G., R. Ford, and R. Hall, *Estimation of toxic hazard—a decision tree approach.* Food

and cosmetics toxicology, 1976. **16**(3): p. 255-276.
32. Munro, I.C., et al., *Correlation of structural class with no-observed-effect levels: a proposal for establishing a threshold of concern.* Food and Chemical Toxicology, 1996. **34**(9): p. 829-867.
33. Patlewicz, G., et al., *An evaluation of the implementation of the Cramer classification scheme in the Toxtree software.* SAR and QSAR in Environmental Research, 2008. **19**(5-6): p. 495-524.
34. Van Der Spoel, D., et al., *GROMACS: fast, flexible, and free.* Journal of computational chemistry, 2005. **26**(16): p. 1701-1718.
35. Best, R.B., et al., *Optimization of the additive CHARMM all-atom protein force field targeting improved sampling of the backbone ϕ, ψ and side-chain $\chi1$ and $\chi2$ dihedral angles.* Journal of chemical theory and computation, 2012. **8**(9): p. 3257-3273.
36. Rivail, L., et al., *Large-scale molecular dynamics of a G protein-coupled receptor, the human 5-HT4 serotonin receptor, in a lipid bilayer*. Journal of Molecular Structure: THEOCHEM, 2007. **817**(1-3): p. 19-26.
37. Vanommeslaeghe, K. and A.D. MacKerell Jr, *Automation of the CHARMM General Force Field (CGenFF) I: bond perception and atom typing.* Journal of chemical information and modeling, 2012. **52**(12): p. 3144-3154.
38. Hess, B., et al., *GROMACS 4: algorithms for highly efficient, load-balanced, and scalable molecular simulation.* Journal of chemical theory and computation, 2008. **4**(3): p. 435-447.
39. Hoover, W.G., *Canonical dynamics: Equilibrium phase-space distributions.* Physical review A, 1985. **31**(3): p. 1695.
40. Nosé, S., *A molecular dynamics method for simulations in the canonical ensemble.* Molecular physics, 1984. **52**(2): p. 255-268.
41. Nosé, S. and M. Klein, *Constant pressure molecular dynamics for molecular systems.* Molecular Physics, 1983. **50**(5): p. 1055-1076.
42. Parrinello, M. and A. Rahman, *Polymorphic transitions in single crystals: A new molecular dynamics method.* Journal of Applied physics, 1981. **52**(12): p. 7182-7190.
43. Darden, T., D. York, and L. Pedersen, *Particle mesh Ewald: An N· log (N) method for Ewald sums in large systems.* The Journal of chemical physics, 1993. **98**(12): p. 10089-10092.
44. Essmann, U., et al., *A smooth particle mesh Ewald method.* The Journal of chemical physics, 1995. **103**(19): p. 8577-8593.
45. Hess, B., et al., *LINCS: a linear constraint solver for molecular simulations.* Journal of computational chemistry, 1997. **18**(12): p. 1463-1472.
46. Siddique, H.R. and M. Saleem, *Beneficial health effects of lupeol triterpene: a review of preclinical studies.* Life sciences, 2011. **88**(7-8): p. 285-293.
47. Ruzicka, L., *The isoprene rule and the biogenesis of terpenic compounds.* Experientia, 1953. **9**(10): p. 357-367.
48. Cheng, S.-Y., et al., *Biological activity of oleanane triterpene derivatives obtained by chemical derivatization.* Molecules, 2013. **18**(10): p. 13003-13019.
49. Kazakova, O. and I. Smirnova. *Antiviral activity of lupane and oleanane A-seco-triterpenoids*. in *AIP Conference Proceedings*. 2022. AIP Publishing LLC.
50. Su, Y., et al., *Design, synthesis of oleanolic acid-saccharide conjugates using click chemistry methodology and study of their anti-influenza activity.* European Journal of Medicinal Chemistry, 2019. **182**: p. 111622.
51. Wu, J., et al., *SZC015, a synthetic oleanolic acid derivative, induces both apoptosis and autophagy in MCF-7 breast cancer cells.* Chemico-biological interactions, 2016. **244**: p. 94-104.
52. Orhan, I.E. and F.S. Senol Deniz, *Natural products as potential leads against coronaviruses: could they be encouraging structural models against SARS-CoV-2?* Natural products and bioprospecting, 2020. **10**(4): p. 171-186.
53. Duric, K., et al., *Antibacterial activity of methanolic extracts, decoction and isolated triterpene products from different parts of birch, Betula pendula, Roth.* Journal of Plant Studies, 2013. **2**(2): p. 61.
54. Feng, J., et al., *Novel triterpenoids and glycosides from durian exert pronounced anti-inflammatory activities.* Food chemistry, 2018. **241**: p. 215-221.
55. Luchnikova, N.A., V.V. Grishko, and I.B. Ivshina, *Biotransformation of oleanane and ursane triterpenic acids.* Molecules, 2020. **25**(23): p. 5526.
56. Das, J., A. Sarkar, and P. Ghosh, *Friedelane triterpenoids: transformations toward A-ring modifications including 2-homo derivatives.* New Journal of Chemistry, 2018. **42**(9): p. 6673-6688.
57. Chang, F.-R., et al., *Anti-human coronavirus (anti-HCoV) triterpenoids from the leaves of Euphorbia neriifolia.* Natural product communications, 2012. **7**(11): p. 1934578X1200701103.

58. Van Doelen, G., *Molecular studies of fresh and aged triterpenoid varnishes*. 1999, Amsterdam.
59. Zhang, X., et al., *Three new hopane-type triterpenoids from the aerial part of Adiantum capillus-veneris and their antimicrobial activities.* Fitoterapia, 2019. **133**: p. 146-149.
60. Liu, J., et al., *Isolation and characterization of new minor triterpenoid saponins from the buds of Lonicera macranthoides.* Carbohydrate research, 2013. **370**: p. 76-81.
61. Marciniec, K., et al., *Phosphate derivatives of 3-carboxyacylbetulin: Synthesis, in vitro anti-HIV and molecular docking study.* Biomolecules, 2020. **10**(8): p. 1148.
62. Huang, H., *The effect of biodegradation on gammacerane in crude oils.* Biodegradation, 2017. **28**(4): p. 313-326.
63. Ikeda, T., et al., *Anti-herpes virus type 1 activity of oleanane-type triterpenoids.* Biological and Pharmaceutical Bulletin, 2005. **28**(9): p. 1779-1781.
64. Huang, W., et al., *Inhibition of intercellular adhesion in herpex simplex virus infection by glycyrrhizin.* Cell biochemistry and biophysics, 2012. **62**(1): p. 137-140.
65. Pompei, R., et al., *Glycyrrhizic acid inhibits virus growth and inactivates virus particles.* Nature, 1979. **281**(5733): p. 689-690.
66. Shanmugam, M.K., et al., *Targeted inhibition of tumor proliferation, survival, and metastasis by pentacyclic triterpenoids: potential role in prevention and therapy of cancer.* Cancer letters, 2012. **320**(2): p. 158-170.
67. Shetty, A.V., et al., *18α-glycyrrhetinic acid targets prostate cancer cells by down-regulating inflammation-related genes.* International journal of oncology, 2011. **39**(3): p. 635-640.
68. Zheng, W., et al., *Glycyrrhizic Acid for COVID-19: Findings of Targeting Pivotal Inflammatory Pathways Triggered by SARS-CoV-2.* Frontiers in Pharmacology, 2021. **12**.
69. Chen, K., et al., *Anti-AIDS agents, 4. Tripterifordin, a novel anti-HIV principle from Tripterygium wilfordii: Isolation and structural elucidation.* Journal of natural products, 1992. **55**(1): p. 88-92.
70. Bache, M., et al., *Increased betulinic acid induced cytotoxicity and radiosensitivity in glioma cells under hypoxic conditions.* Radiation Oncology, 2011. **6**(1): p. 1-9.
71. Paduch, R. and M. Kandefer-Szerszen, *Antitumor and antiviral activity of pentacyclic triterpenes.* Mini-Reviews in Organic Chemistry, 2014. **11**(3): p. 262-268.
72. Santos, R.C., et al., *New betulinic acid derivatives induce potent and selective antiproliferative activity through cell cycle arrest at the S phase and caspase dependent apoptosis in human cancer cells.* Biochimie, 2011. **93**(6): p. 1065-1075.
73. Suresh, C., et al., *New ionic derivatives of betulinic acid as highly potent anti-cancer agents.* Bioorganic & medicinal chemistry letters, 2012. **22**(4): p. 1734-1738.
74. Savita, S., S. Mishra, and K. Jaiswal, *Molecular docking studies of betulinic acid and its structurally modified derivatives as potential inhibitors of COVID-19 main protease protein.* Biochemical and Cellular Archives, 2020: p. 4503-4510.
75. Fukushima, E.O., et al., *CYP716A subfamily members are multifunctional oxidases in triterpenoid biosynthesis.* Plant and Cell Physiology, 2011. **52**(12): p. 2050-2061.
76. Pollier, J. and A. Goossens, *Oleanolic acid.* Phytochemistry, 2012. **77**: p. 10-15.
77. Guinda, Á., M.C. Pérez-Camino, and A. Lanzón, *Supplementation of oils with oleanolic acid from the olive leaf (Olea europaea).* European journal of lipid science and technology, 2004. **106**(1): p. 22-26.
78. Žiberna, L., et al., *Oleanolic acid alters multiple cell signaling pathways: implication in cancer prevention and therapy.* International journal of molecular sciences, 2017. **18**(3): p. 643.
79. Sporn, M.B., et al., *New synthetic triterpenoids: potent agents for prevention and treatment of tissue injury caused by inflammatory and oxidative stress.* Journal of natural products, 2011. **74**(3): p. 537-545.
80. Ayeleso, T.B., M.G. Matumba, and E. Mukwevho, *Oleanolic acid and its derivatives: biological activities and therapeutic potential in chronic diseases.* Molecules, 2017. **22**(11): p. 1915.
81. Zhang, F., et al., *Oleanolic acid and ursolic acid in commercial dried fruits.* Food Science and Technology Research, 2013. **19**(1): p. 113-116.
82. Kalogeropoulos, N., et al., *Nutritional evaluation and bioactive microconstituents (phytosterols, tocopherols, polyphenols, triterpenic acids) in cooked dry legumes usually consumed in the Mediterranean countries.* Food Chemistry, 2010. **121**(3): p. 682-690.
83. Guo, S., et al., *Content variations of triterpenic acid, nucleoside, nucleobase, and sugar in jujube (Ziziphus jujuba) fruit during ripening.* Food Chemistry, 2015. **167**: p. 468-474.
84. Sen, A., *Prophylactic and therapeutic roles of oleanolic acid and its derivatives in several diseases.* World Journal of Clinical Cases, 2020. **8**(10): p. 1767.
85. Reisman, S.A., L.M. Aleksunes, and C.D. Klaassen, *Oleanolic acid activates Nrf2 and*

protects from acetaminophen hepatotoxicity via Nrf2-dependent and Nrf2-independent processes. Biochemical pharmacology, 2009. **77**(7): p. 1273-1282.
86. Wang, X., et al., *Antioxidant activities of oleanolic acid in vitro: possible role of Nrf2 and MAP kinases.* Chemico-biological interactions, 2010. **184**(3): p. 328-337.
87. Klaassen, C.D. and S.A. Reisman, *Nrf2 the rescue: effects of the antioxidative/electrophilic response on the liver.* Toxicology and applied pharmacology, 2010. **244**(1): p. 57-65.
88. Wang, X., et al., *Inhibitory effect of oleanolic acid on hepatocellular carcinoma via ERK–p53-mediated cell cycle arrest and mitochondrial-dependent apoptosis.* Carcinogenesis, 2013. **34**(6): p. 1323-1330.
89. Zhao, X., M. Liu, and D. Li, *Oleanolic acid suppresses the proliferation of lung carcinoma cells by miR-122/Cyclin G1/MEF2D axis.* Molecular and cellular biochemistry, 2015. **400**(1): p. 1-7.
90. Mukherjee, H., et al., *Anti-herpes virus activities of Achyranthes aspera: an Indian ethnomedicine, and its triterpene acid.* Microbiological research, 2013. **168**(4): p. 238-244.
91. Kumar, A., et al., *Identification of phytochemical inhibitors against main protease of COVID-19 using molecular modeling approaches.* Journal of Biomolecular Structure and Dynamics, 2021. **39**(10): p. 3760-3770.
92. Nkeh-Chungag, B.N., et al., *Anti-inflammatory and membrane-stabilizing properties of two semisynthetic derivatives of oleanolic acid.* Inflammation, 2015. **38**(1): p. 61-69.
93. Liu, H., et al., *Computational evaluation of the COVID-19 3c-like protease inhibition mechanism, and drug repurposing screening.* 2020.
94. Wu, C., et al., *Analysis of therapeutic targets for SARS-CoV-2 and discovery of potential drugs by computational methods.* Acta Pharmaceutica Sinica B, 2020. **10**(5): p. 766-788.